Contrib Mineral Petrol (2007) 154:291–308
DOI 10.1007/s00410-007-0194-8

ORIGINAL PAPER

Textural and chemical variation in plagioclase phenocrysts from the 1980 eruptions of Mount St. Helens, USA

Kim Berlo · Jon Blundy · Simon Turner · Chris Hawkesworth

Received: 26 January 2006 / Accepted: 27 February 2007 / Published online: 11 April 2007

Abstract This study presents major- and trace-element chemistry of plagioclase phenocrysts from the 1980 eruptions of Mount St. Helens volcano. Despite the considerable variation in textures and composition of plagioclase phenocrysts, distinct segments have been cross-correlated between crystals. The variation of Sr and Ba concentration in the melt, as calculated from the concentration in the phenocrysts using partition coefficients, suggests the cores and rims crystallised from compositionally different melts offset by the plagioclase crystallisation vector. In both of these melts Sr and Ba are correlated despite the abundance of plagioclase in the 1980 dacites. We propose that rapid crystallisation of plagioclase upon magma ascent caused a shift in melt composition towards lower Sr and higher Ba, as documented in the rims of the phenocrysts. Although the cores of the phenocrysts crystallised at relatively shallow depths, they preserve the Sr and Ba of the deep-seated melts as they ascended from a deeper region. Further magma ascent resulted in microlite nucleation, which is responsible for a similar shift to even lower Sr concentration as observed in the groundmass of post-18 May 1980 samples.

Keywords Mount St. Helens · Plagioclase · Nucleation · Crystallisation · Sr and Ba

Communicated by T.L. Grove.

Electronic supplementary material The online version of this article (doi:10.1007/s00410-007-0194-8) contains supplementary material, which is available to authorized users.

K. Berlo · J. Blundy · C. Hawkesworth
Department of Earth Sciences, University of Bristol,
Wills Memorial Building, Queen's road, BS8 1RJ Bristol, UK

K. Berlo (✉)
Department of Earth and Planetary Sciences, McGill University,
3450 University Street, H3A 2A7 Montreal, QC , Canada
e-mail: Kim_Berlo@inbox.com

S. Turner
GEMOC, Department of Earth and Planetary Sciences,
Macquarie University, Sydney, NSW 2109, Australia

Introduction

The potential of plagioclase as an archive of magmatic processes has long been recognized and exploited (e.g. Stamatelopoulou-Seymour et al. 1990; Blundy and Shimizu 1991; Singer et al. 1995; Tepley et al. 2000; Ginibre et al. 2002). Plagioclase is particularly useful because of its ubiquity, its large stability field, and the preservation of major element compositional variation due to the slow interdiffusion of NaSi–CaAl (Morse 1984). Changes in melt composition recorded by variations in plagioclase composition are the result of pressure, temperature and bulk compositional variation. Smaller compositional variations in plagioclase, e.g. oscillatory zoning, may reflect local kinetic effects at the crystal-melt interface (e.g. Allègre et al. 1981) and do not necessarily imply pressure–temperature–compositional variations in the magmatic system as a whole, which is the focus of this contribution. Pressure, temperature and composition delimit the stability field of plagioclase and variations in these parameters can result in textural features such as resorption, rapid growth and melt/solid inclusion entrapment (e.g. Lofgren 1974a; Tsuchiyama 1985; Nakamura and Shimakita 1998; Hammer and Rutherford 2002).

With the advance of microanalysis techniques for trace elements and isotope ratios the importance of plagioclase as an archive of magma evolution, including magma-

mixing and assimilation, has become even greater. It has been recognised that many crystals that were previously perceived as true phenocrysts did in fact not crystallize from the host melt (e.g. Davidson et al. 2005). Many crystals appear to be recycled in the crust and have seen multiple magmatic episodes, in particular in evolved systems (e.g. Blundy and Shimizu 1991; Gardner et al. 2002). This may explain some of the old ages from crystals obtained from U-series disequilibrium studies (Cooper and Reid 2003; Turner et al. 2003). It also has important implications for the interpretation of whole-rock analyses, because phenocryst-bearing magmas may be mixtures of melt and a phenocryst cargo of variable age and origin such that whole rocks may not represent true liquid compositions. This complication may at first sight appear to reduce the potential of plagioclase as a tracer of magma evolution. However, the complexity and preservation of plagioclase zonation is more likely to enhance its potential by providing information on the evolution of not just one magma batch, but of the magmatic system as a whole. For example, the cores of plagioclase phenocrysts can provide a window into the source region of the magmas (e.g. Bindeman and Bailey 1999). Thus, signals that are obscured by shallow processes in the bulk rock, such as fractional crystallisation, degassing and magma mixing can be retrieved from the dusty corners of the plagioclase archive.

Of course, not all plagioclase phenocrysts are foreign to their present host rock (e.g. Kuritani 1999) and crystal growth studies suggest that crystals can grow from melt on timescales as short as years to days (e.g. Cashman 1988; Geschwind and Rutherford 1995; Pearce et al. 1987). This is corroborated by the fact that crystallisation can also take place in response to decompression and degassing, which can occur on a time scale of days to decades, rather than the much longer time needed for cooling (e.g. up to 10^5 years, Hawkesworth et al. 2000). The crystals that form during degassing are not only microlites, but also include complete phenocrysts and/or rims on existing phenocrysts (e.g. Kuritani 1999; Blundy and Cashman 2001, 2005). Thus, phenocrysts can form in a mixture of environments including deep-seated magma reservoirs, cumulates and wall-rock and the conduit itself. This variety of different origins and processes implies that studies using phenocryst populations rather than individual crystals tend to average, rather than tease out, magmatic processes. This contribution aims to study a large number of phenocrysts from a single well-studied volcano, Mount St. Helens, in an attempt to decipher common magmatic processes through the diversity of the individual crystals. No two crystals are the same, but many share a common history that is recorded in the plagioclase archive in different ways.

As well as crystallising under a variety of conditions crystals can have grown over variable time spans and at different times. At Mount St. Helens, at least part of the plagioclase population, whether individual crystals or parts thereof, has to be relatively old compared to their eruption age (Cooper and Reid 2003). However, it has also been suggested that decompression degassing crystallization played an important role at the Mount St. Helens 1980–1986 eruption (Blundy and Cashman 2001), thus implying young crystals that grew during magma ascent. A previous study of Mount St. Helens plagioclase suggests that more than one phenocryst population is present in the 1980 eruption of Mount St. Helens with overlapping magmatic records (Pearce et al. 1987). This may indicate that crystallisation occurred in distinct stages and that both old and young crystals are preserved within a single rock sample.

Approach

The magmatic history of Mount St. Helens is discussed in detail by Smith and Leeman (1987, 1993), Pallister et al. (1992) and Gardner et al. (1995a, b) amongst others. Smith and Leeman (1987) show that differentiation is likely to occur in the lower crust, where repeated intrusion leads to the formation of H_2O-rich evolved melts by a combination of partial melting and crystallisation (Annen et al. 2006). Magma mixing is apparent (e.g. Gardner et al. 1995a) and may be responsible for cycles in compositional variation with time (Pallister et al. 1992). Given the longevity of plagioclase (Cooper and Reid 2003), crystals in the 1980 eruptions could potentially be inherited from earlier episodes and/or document such processes.

For this study plagioclase phenocrysts from the 18 May eruption, the cryptodome and both previous (Cashman and Hoblitt 2004) and subsequent eruptions during 1980 were used (eruptions on: 13 April, 18 May, 12 June, 22 July, 7 August, 16–18 October). Extensive SEM imaging revealed the scope of the compositional and textural variation in plagioclase crystals. Considering the number of processes that can be responsible for the formation of the different textures and compositions of plagioclase phenocrysts, it is clearly unlikely that the records of magmatic evolution of individual crystals converge towards a single simple magmatic history. For that reason this study focuses on a substantial subset of distinctive textures that recur in every sample we have studied and which have overlapping zoning. This approach implies that there are other crystals, e.g. microlites, which may have recorded different stages of the evolution of the magmatic system. As a reference dataset a limited number of crystals from pre-1980 eruptions were also analysed.

Both plagioclase composition and texture are dependent on multiple variables: pressure, temperature, magma composition, and H_2O content. A persistent challenge in

plagioclase zoning studies is distinguishing between those aspects of the zoning that result from changes in melt composition (open or closed system) and those that result solely from changes in intensive variables. In this study we use trace element data to distinguish between these two competing controls.

Methods

For the 1980 samples over 250 back-scattered electron images were collected using a Hitachi SEM with an average of 20 crystals per sample. The images were acquired at 20 kV, varying the brightness and contrast to accentuate the textures in individual grains. Roughly 60 crystals were selected for wave-length dispersive electron microprobe analysis (EMP). These analyses were done using either a JEOL JXA-8600 or a Cameca SX-100 probe at the University of Bristol, with an accelerating voltage of 20 kV and 10 nA beam current with a 5 μm defocused beam. For most of the selected crystals core-rim profiles were analysed; for others only spot analyses representing different textural components were made. Calibration was based on the following standards: wollastonite (Si, Ca), albite (Na, Al), olivine (Fe) and orthoclase (K). Peak count times were 20 s for Na, Al and Si, 30 s for K and Ca, and 60 s for Fe; background counting times were 10 or 15 s.

Based on the combined SEM and EMP data, 30 crystals from the 1980 eruptions were selected for secondary ion mass spectrometry (SIMS). Trace elements were determined by SIMS on Au-coated thin sections and grain mounts using a Cameca IMS-4f ion-microprobe at the University of Edinburgh. The primary beam was 10 keV (nominal) O^- ions. The secondary ion accelerating voltage was 4.5 kV with an offset of 75 V and an energy window of ±20 eV to reduce molecular ion transmission on the masses of interest. For profile analyses we operated with a sample current of 5 nA corresponding to spatial resolution of ~6–12 μm diameter; for spot analyses we increased the beam current to 10 nA resulting in a spatial resolution of 20–25 μm diameter. Calibration was performed on NIST glass SRM 610 under similar operating conditions. ^{26}Mg, ^{47}Ti, ^{88}Sr, ^{138}Ba were measured and ratioed to ^{30}Si as determined from subsequent EMP analysis of SiO_2 in an area near the SIMS spot. To account for small differences in ion-yield between feldspar and NIST glass, we adopted the following correction factors based on repeat analyses of Lake County Labradorite (Mg/0.881; Ti/0.793; Sr/0.796; Ba/0.773). Analytical count times were adjusted so as to ensure a statistical precision of better than 2% relative for all isotopes. The accuracy of SIMS data for Sr and Ba, assessed by analysis of Sapphire Hills Anorthoclase (SHF 1; Irving and Frey 1984) as a secondary standard under similar operating conditions, is better than 5 and 10% relative, respectively. Part of the dataset was published by Berlo et al. (2004).

For 18 crystals rim-to-core profiles were analysed, for 1 crystal rim-to-rim profiles in perpendicular directions and for 14 crystals only spot analyses were made. The crystals were not oriented, because of difficulties with the often broken nature of the crystals and because most are in thin sections. Along with the plagioclase phenocryst analyses a limited number of groundmass glasses, melt inclusions and microlites were analysed for trace elements. As well as this extensive dataset for 1980 plagioclase a smaller subset of point analyses on two different basalts from the Castle Creek period, a rhyodacite from the Sugar Bowl period, and a single profile along a plagioclase crystal from a Goat Rocks andesite were obtained (see online data file).

In-situ $^{87}Sr/^{86}Sr$ ratios of 8 selected plagioclase crystals of the 18 May and 7 August eruptions were determined by LAM-MC-ICPMS at Macquarie University. The laser ablation microprobe was a New Wave UP213 system connected to a Nu Plasma MC-ICPMS (Nu005). Laser operating conditions included a repetition rate of 4 Hz, a beam aperture size of 60–70 μm and a fluence of 33.08 J/cm^2. The ablation was performed in pure He and the He-sample aerosol was mixed with Ar prior to introduction into the ICP. Masses 83 through 88 were collected in Faraday cups using a static collection mode. Interference of ^{87}Rb on ^{87}Sr was corrected using the intensity of ^{85}Rb following Macquarie University protocols (Adams et al. 2005). A 60s background was measured on peak before each analysis to account for the Kr interferences on ^{84}Sr and ^{86}Sr. Accuracy based on repeat analysis of the Batbjerg clinopyroxene standard is better than 0.00003 absolute and precision is better than 0.0001 (2 SD). To allow long counting times and thus reduce the error on individual analyses with minimal risk of drilling into different (deeper) zones, troughs parallel to the zoning profiles were analysed.

Plagioclase texture and chemistry

We have concentrated on phenocrysts with diameters between 400 and 1,000 μm. Microphenocrysts, microlites and larger xenocrysts are touched on briefly, but not studied in detail: a detailed study of microlites was performed by Cashman (1988, 1992). Three main types of phenocrysts with different core textures (A, B, C), but similar rim features were observed (Figs. 1, 2). These crystals have been divided into zones, numbered inwards from rim to core (1–8), each with distinct major and trace element composition and texture. The zones are characterised by roughly homogeneous compositions (despite small variations and minor resorption surfaces) and boun-

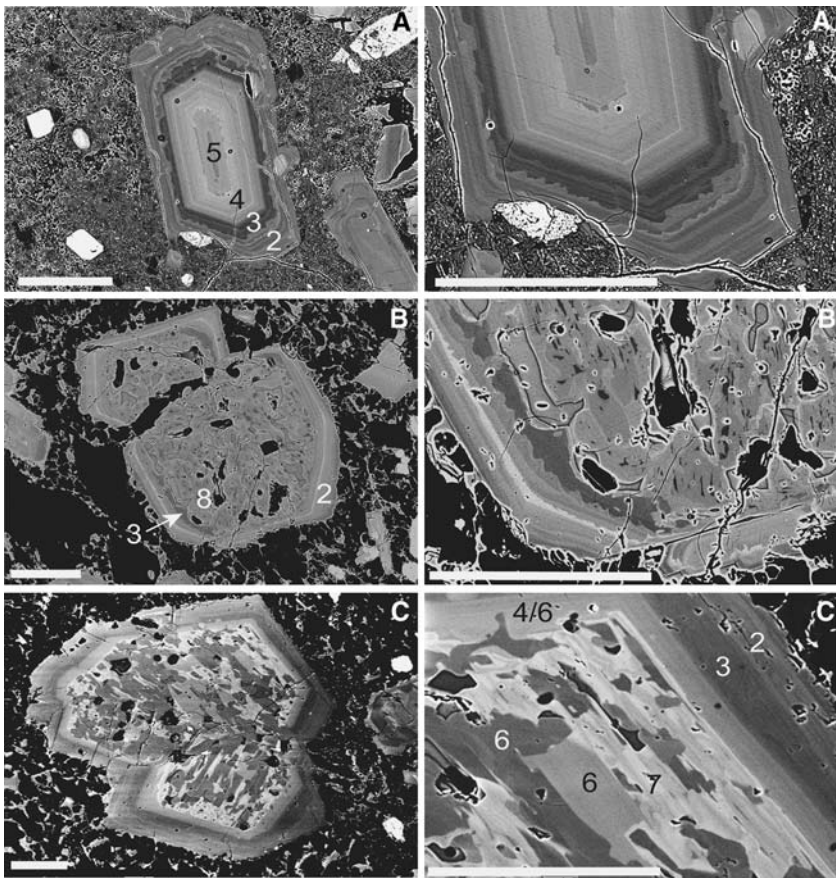

Fig. 1 Back-scattered electron images of examples of type *A*, normal texture, type *B*, spongy cellular texture and type *C*, boxy cellular texture, plagioclases. For details on different textures see text. The scale bar is 200 μm in every image and the *numbers* refer to zones of similar texture and composition that are identifiable in multiple phenocrysts (Fig. 3)

ded by major shifts in composition. Some of the zones can be found in all three types of crystals, although they may not have formed or were not preserved in every individual crystal. Other zones are unique to a particular type of crystal. A summary of these zones is given in Fig. 3 and the three main phenocryst types are discussed below.

Type A: phenocrysts with An_{60} cores

Type A phenocrysts (Fig. 1) are characterised by broad homogeneous cores of roughly An_{60} composition (these appear similar to ''Type 1 phenocrysts'' of Pearce et al. 1987). The cores sometimes have a resorbed more sodic centre. The An_{60} core is called zone 4, its resorbed centre zone 5. Surrounding the cores is an oscillatory-zoned mantle of roughly An_{40} composition, referred to as zone 3. The transition from zone 4 (An_{60} core) to zone 3 (An_{40} mantle) is gradual, but relatively sharp. There is no clear indication of resorption at this boundary. The rims of type A crystals (zone 2) are more calcic with roughly An_{50} and oscillatory zoning. The boundary between zones 2 and 3 is characterised by resorption. The outermost 10–20 μm of the phenocrysts has been designated zone 1; its boundary with zone 2 is a resorption surface. Despite recording the last stage of magma evolution zone 1 is not the same in every crystal.

Figure 2 shows the major and trace element variation along rim to core profiles in individual crystals. Note that not all crystals have exactly the same sequence of zones (1-2-3-4-5), as some crystals have missing zones either due to non-formation or non-preservation. Exact correlation of zoning features within zones, e.g. small resorption features or Ca-spikes, is not possible (see also Pearce et al. 1987). The zones defined above do not only have similar major element composition and textures, their trace element chemistry can also be correlated between crystals (Fig. 2). Zones 4 and 5 (the core) have very similar trace element compositions. Sr concentrations in the core are generally the highest, while Ba concentrations are the lowest. Figure 4 shows the variation in Sr–Ba for individual zones. Zone 3 has the highest Ba concentration and the transition from zone 4 to 3 is usually accompanied by a drop in Sr. Mg and Ti concentrations also tend to be lower in zone 3 than in zones 4 and 5 (Fig. 2). The rim (zones 1 and 2) has distinctly higher Mg and to lesser extent Ti than the core and the mantle. Ba concentrations are intermediate between core and mantle.

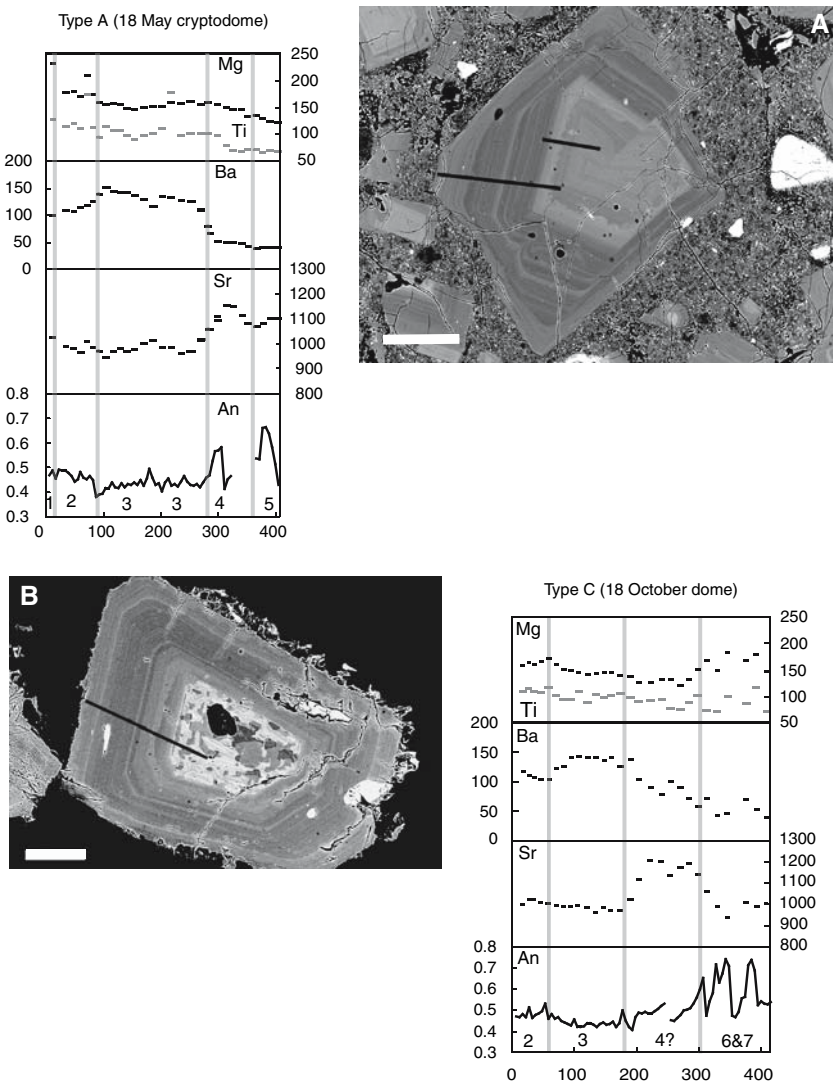

Fig. 2 Rim to core profiles through four phenocrysts erupted during 1980 for An (mol %) and trace elements (ppm). A further eight profiles can be found in a supplementary data file. The *profile lines* are shown in adjacent BSE images. Individual phenocrysts have been compared to distinguish zones of similar composition, chemistry and texture (*numbers* refer to crystal zones as indicated in Fig. 3). The width of each trace element point corresponds to the size of the SIMS pit

Type B: spongy cellular cores

These crystals have different cores than type A crystals (Fig. 1), but their rims have similar zones. The cores have a rounded sponge-like texture with many large (<100 μm) melt inclusions, which appear to form an interconnected network. The cores have a heterogeneous appearance with rounded smaller patches of compositionally different plagioclase. Around the melt inclusions there are often thin rims of calcic plagioclase, which appear to outline the full extent of the melt inclusion before post-entrapment crystallisation (e.g. Stewart and Pearce 2004; Blundy et al. 2006). The apparent network of melt inclusions was also noted by Pearce et al. (1987) and described in Mount Meager volcanic rocks by Stewart and Pearce (2004). In some cases thin capillaries extending over 200 μm connect melt inclusions in the core of a crystal with the matrix glass. These capillaries appear to have remained open while the crystal was in the process of growing an almost melt-inclusion-free rim. Plagioclase zoning around the entrance of the melt inclusion network bends inwards suggesting crystallisation on the walls of the channel, rather than on the contact with the matrix. Thus it is suggested that these melt inclusions have remained open systems until the network was sealed off either by crystallisation of part of the channels or by formation of a continuous rim around the crystal. Melt inclusion studies have shown that they were connected to the melt until very shortly before, or even during, eruption (Blundy and Cashman 2005; Berlo et al. 2004; Blundy et al. 2006), thus recording changes in the melt during magma ascent. Although most melt inclusions are rounded, some show evidence of plagioclase growth from the melt inclusion giving them an angular appearance in detail. Most do not contain microlites, but some fragmented crystals do.

Fig. 2 continued

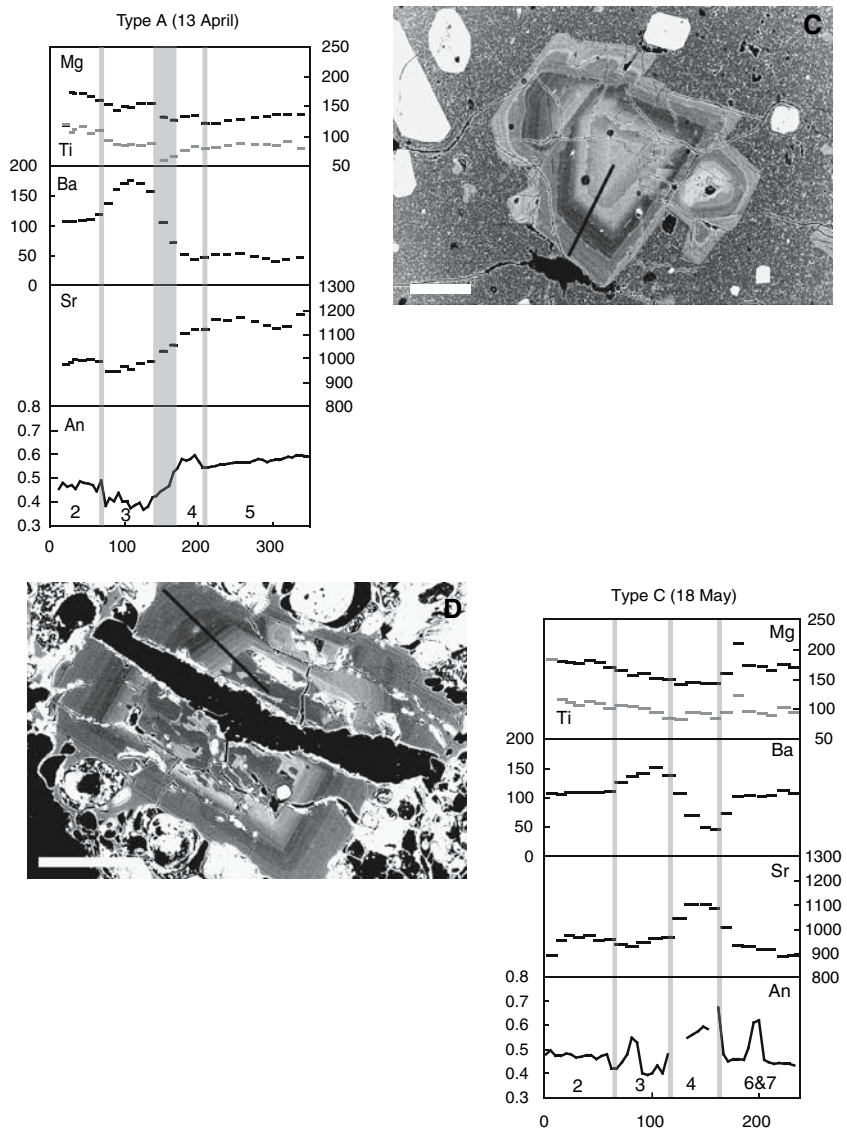

The inhomogeneous core of type B crystals has been designated zone 8 (Fig. 3). The heterogeneity consists of the remains of the pre-existing plagioclase, thin calcic spikes outlining the original extent of resorption and newly grown plagioclase that crystallised from the melt channels while in connection with the groundmass. Often it is not possible to analyse these features separately by EMP or SIMS, resulting in hybrid analyses. The overall composition of these cores usually lies between An_{45} and An_{50}. Core boundaries are usually rounded and diffuse, characterised by a resorption surface and sometimes a Ca peak. Some spongy crystals have part of zone 3 mantle, while others only have a zone 2 rim. The resorption that caused the spongy textures appears to be correlated with the resorption between zones 3 and 2 in type A crystals.

Ba concentrations of the zone 8 cores (keeping in mind that these are probably hybrid analyses) are similar to zones 3 and 2. Sr concentrations are slightly lower than in the rim (Fig. 4). Contrary to type A and type C crystals, type B crystals have high Ba concentration in both core and rim, while type A and type C have lower Ba concentration in the core and high Ba concentration in the rim. Ti concentrations are similar to those in zone 2 and 3, but the Mg concentrations are generally higher than in zones 3 and 4, but not to the same degree as the rim.

Type C: boxy cellular cores

As with type B these crystals display a different core texture, but the rim contains the same zones as type A. Boxy cellular cores display a chessboard-like pattern of anorthite-rich ($An_{67–82}$) and anorthite-poor ($An_{47–54}$) patches (e.g. Figs. 1, 2). The boundaries between the patches are usually straight, suggesting that they are controlled crystallographically. In detail, the patches are not homogeneous

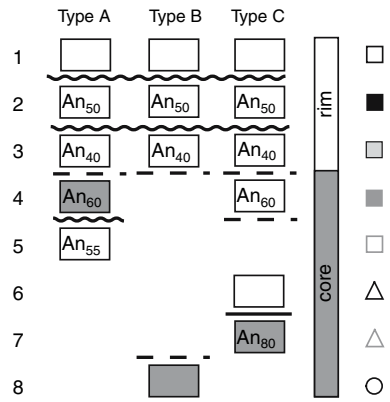

Fig. 3 Schematic table of characteristics of type *A*, *B* and *C* phenocrysts and the division of zones. Zones 1–3 are rim zones that may be present in all types, zones 4–8 are core zones that are characteristic for each specific crystal type. The zones characteristic of individual phenocrysts types are indicated in *grey*. Typical composition of zones are indicated in the *boxes*, *open boxes* indicate variable composition. The boundaries between zones can be resorbed (*wavy line*), gradational (*dashed line*) or sharp (*straight line*). The *symbols* on the right hand side denote those used in Figs. 4 and 9c

(Fig. 1c). Anorthite-rich patches have very fine lines of more sodic plagioclase, which are sometimes cut off by the anorthite-poor patches. These patches are more homogeneous, but do sometimes show a broader type of zoning that is in turn cut by the anorthite-rich patches. The composition of the anorthite-poor patches is also bimodal (~An_{47} and ~An_{54}). It appears that the anorthite-poor patches represent plagioclase crystallised from the same melt as the rim, i.e. melt has invaded an open channel network in a pre-existing skeletal anorthite-rich plagioclase. The compositions of the first and second rim around the core

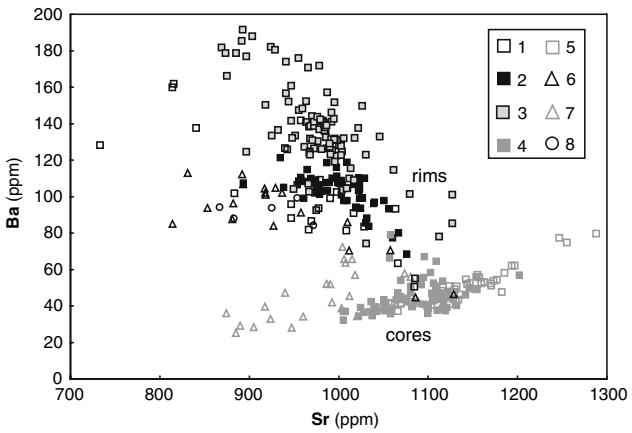

Fig. 4 Sr versus Ba concentrations in plagioclase for correlated zones, see (Figs. 1, 3) and text for characteristics of zones. In general *cores* have low Ba concentration (except type B, zone 8), whereas *mantles* and *rims* have higher Ba concentrations

are both present within the core itself as anorthite-poor patches. Often small angular melt inclusions are trapped on the boundary between An-rich and An-poor patches.

Boxy cellular texture is also observed as a rim around less calcic cores which appear to be frozen in the process of resorption and precipitation of calcic plagioclase (Supplementary file). This process does not only occur on the surface of the crystals but often progresses along cracks towards the centre. Crystals with very calcic boxy rims could represent different sections of the same crystals that only display boxy cellular cores, without pre-existing plagioclase. If this is the case then an older pre-existing type of plagioclase may be present in some of the boxy cellular cores, in addition to embayments of the rim plagioclase.

Type C cores are assigned two zones: zone 6 for the An-poor infill and zone 7 for the An-rich skeleton. The trace element chemistry of zone 7 is different from all the other zones; it has the lowest Ba, low Sr, high Ti and the highest Mg. The variation among the boxy cores themselves is large. Zone 6 has a trace element chemistry similar to that of the type B cores and thus similar to the mantle (zone 3) and rim (zone 2). The boundary of type C cores is usually sharp and can be near euhedral in outline. Surrounding the core is plagioclase that is similar to some of the sodic patches in the core (zone 2), but can also resemble zones 4 (core of type A). Boxy cellular cores are surrounded by rims of zone 3, 2 and sometimes an outermost rim zone 1.

General trends in plagioclase major- and trace-elements

Plagioclase compositions from the 1980 eruptions range from An_{30} to An_{82} and cover broadly the same range as in previous eruptions (Fig. 5). Figure 6 shows peaks at An_{47} and An_{60}, which roughly correspond to average core (zones 4-5-6-7-8) and average rim compositions (zones 3-2-1). Despite the large number of analyses this histogram is not statistically fully representative, as most analyses are along profiles, which were only conducted on plagioclases with few inclusions and other heterogeneities (mainly type A crystals). Thus spongy (type B) and boxy cellular (type C) crystals are underrepresented, although they are less common than normal type A crystals.

The variation in Sr and Ba concentration in plagioclase is depicted in Fig. 4. Most notable in this plot is the apparent lack of data at intermediate Ba concentrations (40–80 ppm): cores generally have low Ba content, whereas rims have higher Ba concentrations, with relatively few data bridging the gap in between. Thus a similar bimodality is present in the Ba data as in the major element composition that distinguishes cores and rims.

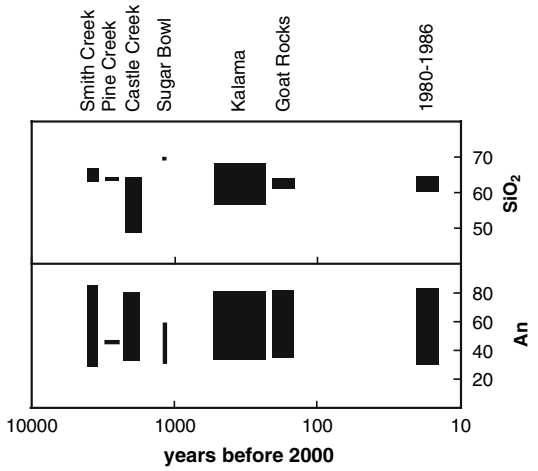

Fig. 5 Compositional variation in bulk rocks and plagioclase over time at Mount St. Helens. Although bulk rock compositional variation in eruptive periods is limited, plagioclase composition varies widely. Data sources for bulk rocks: Smith and Leeman (1987, 1993), Gardner et al. (1995a), Pallister et al. (1992), Melson (1983), Criswell (1987), Cashman and Taggart (1983), and for the plagioclase: Smith (1984), Cooper and Reid (2003), Gardner et al. (1995a), and this study. Note that the limited range of plagioclase composition during Pine Creek period (<3,000 years ago) in this diagram is caused by insufficient data

Sr-isotopes

The results of the Sr isotope analyses are shown in Table 1. The size of the laser beam and the need for trough analyses, inhibited the analysis of distinct zones. Thus, the analyses have been divided into core (zones 4–5) and rim (zones 2–3), and, where possible, mantle (zone 3). For the same reason only cores of type A phenocrysts were analysed. Although there appears to be some variation in $^{87}Sr/^{86}Sr$, both within crystals and between crystals this is mostly within 2 SD (Table 1). The population is therefore relatively homogeneous within the precision of the method. Where individual crystals have different core and rim isotopic compositions rims are not consistently more radiogenic than cores or vice versa (Table 1).

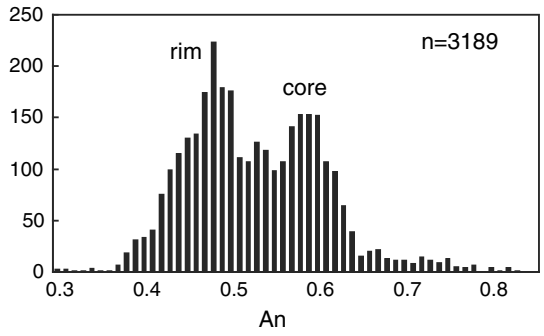

Fig. 6 The distribution of plagioclase compositions in 1980 eruptions is bimodal with peaks at An_{47} and around An_{60}, which correspond roughly to the rims and cores of most phenocrysts. The total number of analyses is 3,189.

Table 1 $^{87}Sr/^{86}Sr$ for 8 phenocrysts from the 18 May and 7 August eruptions with the error (250) in brackets

	An	$^{87}Sr/^{86}Sr$
Rim	0.53	0.70348 (26)
Core	0.53	0.70358 (36)
Core	0.56	0.70332 (26)
Core	0.54	0.70357 (8)
Core	0.64	0.70357 (8)
Mantle	0.40	0.70337 (9)
Rim	0.50	0.70347 (11)
Rim	0.49	0.70382 (12)
Mantle	0.46	0.70343 (13)
Core	0.53	0.70364 (26)
Core	0.53	0.70371 (22)
Mantle	0.50	0.70394 (18)
Rim	0.51	0.70352 (11)
Rim	0.50	0.70380 (9)
Core	0.54	0.70365 (6)
Rim	0.50	0.70353 (5)
Core	0.71	0.70364 (7)
Core	0.63	0.70380 (10)
Mantle	0.44	0.70360 (6)
Rim	0.51	0.70366 (7)
Core	0.65	0.70354 (5)
Core	0.43	0.70360 (10)
Rim	0.53	0.70348 (7)
Mantle	0.70	0.70375 (12)
Rim	0.52	0.70350 (11)
Rim	0.52	0.70338 (20)
Core	0.61	0.70354 (22)
Mantle	0.62	0.70335 (12)
Mantle	0.70	0.70374 (14)

Table 2 Groundmass and melt inclusion glasses from the 18 May and 7 August eruptions

Eruption date	Glass type	SiO_2	Sr	Ba	Mg	Ti
18 May	Groundmass	71	204	402	3,264	1,728
18 May	Melt inclusion	71	262	431	2,176	1,260
7 August	Groundmass	76	48	440	1,324	2,272
7 August	Groundmass	76	79	420	1,228	1,927
7 August	Melt inclusion	73	59	414	2,275	1,838
7 August	Melt inclusion	74	57	433	2,735	1,884

Table 3 Apparent partition coefficients from 18 May and 7 August

Eruption date	An	D_{Sr}	D_{Ba}	D_{Mg}	D_{Ti}
18 May	0.50	4.71	0.27	0.06	0.08
18 May	0.48	4.64	0.24	0.06	0.07
18 May	0.54	4.12	0.34	0.17	0.22
18 May	0.48	4.38	0.27	0.09	0.11
18 May	0.48	4.60	0.25	0.06	0.07
7 August	0.50	18.2	0.27	0.18	0.10
7 August	0.45	18.6	0.33	0.12	0.12
7 August	0.43	20.7	0.30	0.26	0.11
7 August	0.48	19.7	0.21	0.14	0.05
7 August	0.59	20.8	0.08	0.13	0.05
7 August	0.60	23.4	0.08	0.09	0.03
7 August	0.57	20.2	0.19	0.23	0.08
7 August	0.52	20.4	0.21	0.14	0.05
7 August	0.52	19.7	0.29	0.18	0.06
7 August	0.46	18.5	0.23	0.13	0.05
7 August	0.47	15.3	0.29	0.14	0.05

Plagioclase phenocrysts from older eruptions

The crystals from older deposits have not been studied in as much detail as the 1980 crystals, and only a limited number of analyses were conducted to provide a reference dataset (Fig. 7). The data reported here include two basalts (Cave and pre-Cave) from the Castle Creek period, a rhyodacite from the Sugar Bowl period and an andesite from the Goat Rocks period. An overview of the eruptive history of Mount St. Helens is provided by Pallister et al. (1992) and others (e.g. Smith and Leeman 1987, 1993; Gardner et al. 1995a, b). The analyses also include two microlite analyses from the basalts. The textures observed in the 1980 plagioclase crystals are also present in older deposits. Some crystals in the Goat Rocks andesite and Sugar Bowl rhyodacite show striking resemblances to each other and the 1980 plagioclase not just in core texture, but also in rim zones. A Ca-spike similar to that in the outermost rim of some of the 1980 crystals is also observed in some of the crystals from older deposits where this spike is usually more pronounced.

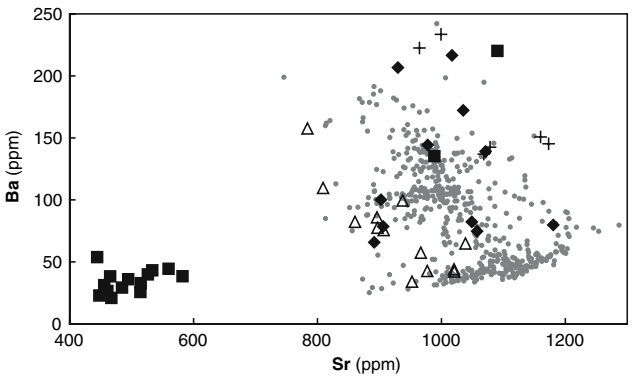

Fig. 7 Sr–Ba variation (in ppm) in plagioclase from pre-1980 eruptions compared to 1980 plagioclase (*grey circles*). *Filled squares* and *diamonds* are in basalts from Castle Creek (Cave and pre-Cave, respectively), *plus* signs are Sugar Bowl dacite and *triangles* are Goat Rocks andesite. The number of analyses of 1980 plagioclase is higher here than in Figs. 4 and 9, because not every single analysis could be assigned unequivocally to a certain zone

The range of Sr and Ba concentrations in plagioclase in the older eruptions is similar to that in the 1980 crystals, except for the crystals of the Cave basalt (Fig. 7). These crystals have cores and rims with only 450–580 ppm Sr (Ba: 20–50 ppm), but their sodic mantles have ~1,000 ppm Sr in line with the mantles of other crystals. The Sr concentration of a Goat Rocks andesite crystal is generally low, but within the range of 1980. Sugar Bowl crystals have higher Sr and Ba concentrations, but again within the 1980 range. Mg and Ti concentrations are higher in both of the basalts and in the andesite and lower in the rhyodacite.

Melt evolution

The trace element chemistry of plagioclase is related to that of the melt from which it grew via the plagioclase-melt partition coefficients for the trace elements of interest. Thus, in order to relate the plagioclase archive to actual magmatic processes, the partition coefficients between plagioclase and melt need to be known. So as to maximise the accuracy of this approach it is essential to apply the partition coefficients that are most suitable to the problem being addressed. It is also important to bear in mind that any diffusion which has occurred after the crystal first grew will tend to blur the information obtained in this way.

The choice of partition coefficients

Sr–Ba

Blundy and Wood (1991) used experimental and natural data from a wide variety of plagioclase and melt compositions to derive the following expressions for the partitioning of Sr and Ba between plagioclase and melt:

$$RT \ln D_{Sr} = 26{,}800 - 26{,}700X_{An} \quad (1a)$$

$$RT \ln D_{Ba} = 10{,}200 - 38{,}200X_{An} \quad (1b)$$

In which R is the ideal gas constant (8.3145 $Jmol^{-1}$ K^{-1}) and temperature (T) is in K. Bindeman et al. (1998) ex-

tended this approach to include a wide range of other trace elements. The relationship they derived for the partitioning of Sr and Ba differs slightly from that of Blundy and Wood (1991):

$$RT \ln D_{Sr} = 28{,}500 - 30{,}400X_{An} \quad (2a)$$

$$RT \ln D_{Ba} = 19{,}100 - 55{,}000X_{An} \quad (2b)$$

To check the applicability of these two sets of expressions to Mount St. Helens plagioclase a comparison between calculated and measured D's (Tables 2, 3) is shown in Fig. 8. Only those plagioclase analyses where the outermost 10 μm of the crystal and the matrix glass were analysed were used to calculate these D's. Unfortunately it was not always possible to analyse the melt composition directly next to such sites due to the glass-poor nature of the samples, their vesicularity and the presence of fractures. Thus the most reliable measurements of partition coefficients come from phenocrysts in the microlite-free 18 May Plinian pumice.

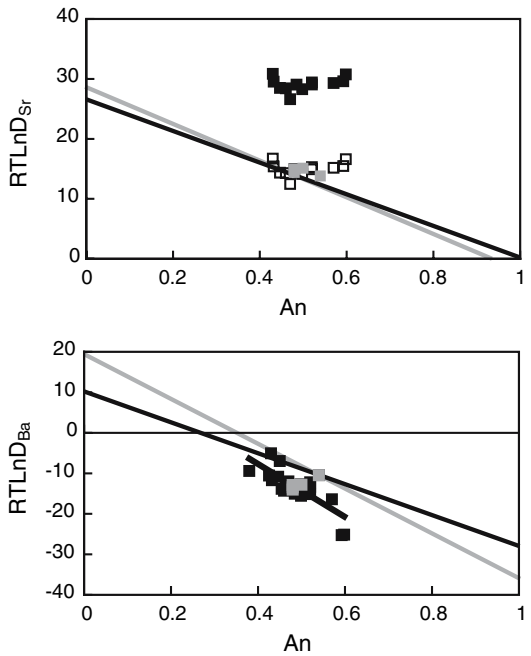

Fig. 8 The Blundy and Wood (1991, *black line*) and Bindeman et al. (1998, *grey line*) expressions for Sr and Ba partition coefficients in plagioclase compared with measured apparent partition coefficients at Mount St. Helens. *Grey squares* are apparent partition coefficient for the microlites-free sample from 18 May 1980 eruption. *Filled squares* are Mount St. Helens apparent partition coefficients for the August 1980 eruption (melt composition can be found in Table 2). *Open squares* are apparent D's when assuming all plagioclase is in equilibrium with 18 May groundmass glass. A best fit line for all Mount St. Helens apparent Ba partition coefficients is also shown (Eq. 3)

The observed Ba partition coefficients are systematically lower than predicted from either model. This suggests that there may be other factor(s) contributing to Ba partitioning, e.g. variations in melt composition or pressure. The effect of pressure on Sr partitioning was determined by Vander Auwera et al. (2000). Their results suggest that a pressure effect may exist, but it is expected to be very small; if the plagioclase phenocrysts crystallized at 1 GPa this would lead to a 10–40 ppm increase in the calculated Sr concentration in the melt compared to the Blundy and Wood (1991) equation (Vander Auwera et al. 2000). It may be that a similarly small pressure effect applies to D_{Ba}, but such effects are probably negligible compared to uncertainties in temperature, major element composition and SIMS analysis. The calculated Ba contents of the melt would plot systematically lower than any measured bulk rock or glass composition, except for one basalt analysis (Smith and Leeman 1993), if either the Blundy and Wood (1991) or the Bindeman et al. (1998) equations are used to calculate melt compositions. This would suggest that none of the crystals, including microlite crystals, crystallised from the 1980 dacites or their predecessors. This was deemed unrealistic and so we have used a modified relation between D_{Ba} and X_{An}, based upon the apparent (measured) D's at Mount St. Helens (see Fig. 8).

$$RT \ln D_{Ba} = 18{,}454 - 65{,}393X_{An} \quad (3)$$

For Sr most of the apparent partition coefficients are much higher than expected from either the Bindeman et al. (1998) or the Blundy and Wood (1991) equations (Fig. 8a). The three data points that do agree with estimated partition coefficients are from the microlite-free 18 May eruption pumice. The microlite-bearing samples are characterised by very low Sr contents in the melt, rather than elevated Sr in the plagioclase (Table 2). This is consistent with rapid depletion of Sr in the melt due to microlites growth, such that only the outermost rim of plagioclase from the August sample records the equilibrium Sr content. This outermost rim is too thin to analyse by SIMS. An analysis located a little further from the contact between plagioclase and melt will thus record the Sr content in equilibrium with a melt prior to crystallisation of the rim. As plagioclase is by far the most dominant crystallising phase, and the rim is volumetrically significant, this will lead to an apparent D_{Sr} which is significantly greater than the true D_{Sr}. Therefore, when the microlite-free groundmass of the 18 May eruption is used to calculate a partition coefficient for the August sample, the calculated values do agree with the modelled ones (Fig. 8). Microlite growth will have little effect on measured D_{Ba}, because a small amount of plagioclase crystallisation will not change the melt concentration of an incompatible element such as Ba significantly.

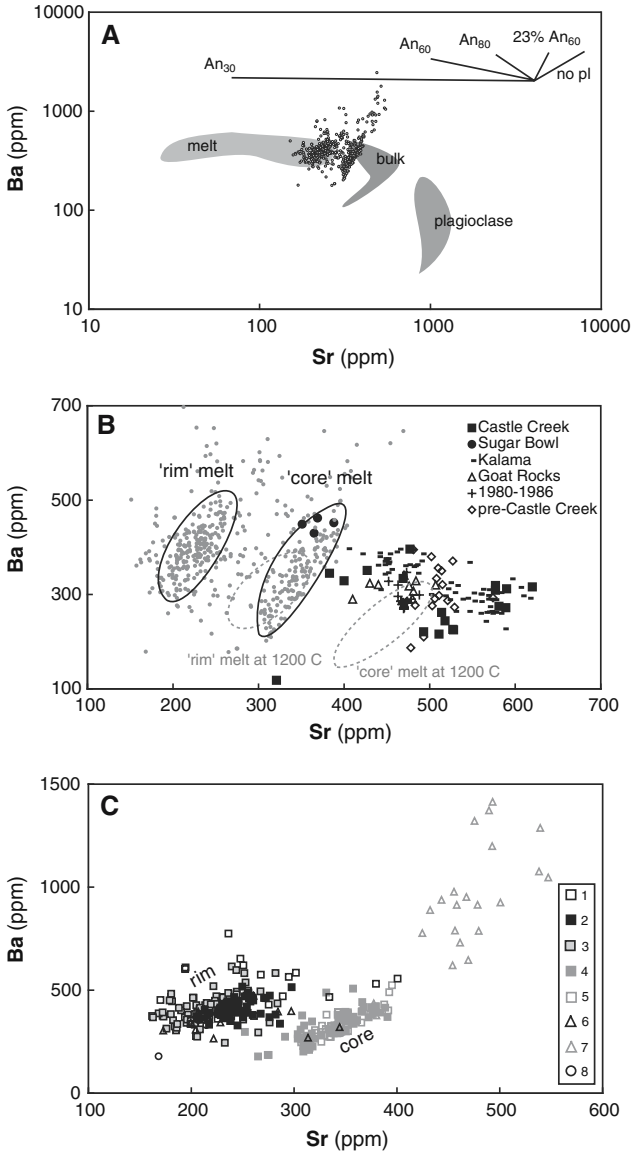

◀ **Fig. 9** Calculated melt Sr and Ba concentrations at 900°C (for details on the calculation see text). **a** Calculated melt composition shown with *small circles* together with *fields* for glass compositions (1980 eruptions of Mount St. Helens; Blundy and Cashman 2005; Blundy et al. 2007; unpublished data), bulk rocks (Pallister et al. 1992; Smith and Leeman 1987, 1993; Gardner et al. 1995a, b; Halliday et al. 1983; unpublished data) and plagioclase (this study). *Vectors* in the upper right corner show the directions of melt evolution for 50% fractional crystallisation of different phases. For most other phases, like pyroxenes, olivine and garnet, $D_{Sr} \approx 0$, which is insignificant compared to plagioclase, resulting in a positive slope for differentiation involving plagioclase-poor assemblages. Note the logarithmic scale. **b** Sr–Ba variation in Mount St. Helens bulk rocks (Pallister et al. 1992; Smith and Leeman 1987, 1993; Gardner et al. 1995a; Halliday et al. 1983; unpublished data) compared to that of the calculated melts at 900°C (in *grey*). Note the gap between melts calculated from the cores of plagioclase phenocrysts (''core-melts'') and those from the mantle and rims (''rim-melts''). The *grey dashed fields* show the Sr and Ba concentration of the same melts calculated at 1,200°C. **c** Calculated melt compositions for individual zones in crystals (Fig. 3). Type A cores (zone 4) grew from a higher Sr melt than the mantles and rims (zones 3, 2 and 1), but both appear to have the same trend to higher Sr and Ba. The An-rich component of type C cores (zone 7) appears to have grown from extremely Ba-rich melts

Although we cannot rule out disequilibrium partitioning as a cause of overestimation of D_{Sr} (e.g. Albarède and Bottinga 1972; Morgan and London, 2003) we consider microlite-induced depletion of the melt the most likely cause of the high measured D_{Sr} and adopt Eq. 1a.

Discussion

Crystal growth and melt evolution

In Fig. 9 and Eqs. 1a and 3 have been used to calculate melt compositions for Sr and Ba, respectively, coexisting with plagioclase. The temperature used in the expressions was 900°C (Rutherford and Hill 1993). The calculated melt compositions straddle the most Sr-rich groundmass and inclusion glasses (Blundy et al. 2007) and the Sr poor end of the bulk rock compositions (i.e. Sugar Bowl rhyodacites; Pallister et al. 1992; Smith and Leeman 1987, 1993; Gardner et al. 1995a, b; Halliday et al. 1983; and unpublished data).

Figure 9a–c shows that the calculated melts define two groups separated by a break in composition, as previously noted for the plagioclase compositions themselves (Fig. 4). The first group corresponds to the core of type A crystals (zones 4 and 5), while the second group corresponds to the mantle/rim (zones 2 and 3) of all crystal types and the core of type B crystals (zones 6 and 8). In the subsequent discussion we will refer to these as ''core-melts'' and ''rim-melts'', respectively. Both groups form parallel trends with positive slopes. In contrast, zone 7 (type C cores) forms an entirely separate group (Fig. 9c) displaced to very high concentrations of Ba (500–1,500 ppm) and Sr (400–550 ppm).

Type *A* phenocrysts

The melts from which the homogeneous cores of type *A* crystals (zone 4), together with their resorbed centres (zone 5), crystallised form a trend towards higher Sr and Ba, suggesting that both elements had similar bulk partition coefficients ($D_{Sr}^{bulk} \approx D_{Ba}^{bulk}$), during this stage of crystallisation. Figure 9a shows that assuming negligible Sr uptake by other phases (e.g. pyroxenes and amphibole) compared to plagioclase, the maximum amount of plagioclase (An_{60}) in the crystallising assemblage at this stage is 23% (the

amount would be less for more sodic plagioclase). The transition to the mantle (zone 3) involves a rather dramatic shift to high Ba and lower Sr concentrations which is accomplished over a relatively small distance in the profile (Fig. 2) and without evidence for significant resorption. In the melt plot (Fig. 9a–c) this shift is manifest as the marked gap between the core and rim-melts.

One way to account for the gap between 'core' and 'rim' melts is a temperature increase during crystallisation of the phenocrysts, for instance as a result of latent heat of crystallisation from the cores. Calculated 'core' and 'rim' melts overlap only if the rims of the phenocrysts crystallised after a temperature increase of 300. Such a temperature increase is well in excess of the likely latent heat of crystallisation (Couch et al. 2003a; Blundy et al. 2006). Moreover a temperature increase would entail resorption of the cores, which is only observed in a few cases, as well as a shift to higher instead of lower An.

We propose instead that the core and rim-melts are chemically distinct. They appear to have been generated by crystallising a similar plagioclase-poor assemblage, because they are nearly parallel, but with the rim-melts displaced to lower Sr and slightly higher Ba than the core-melts (Fig. 9b). Thus we have an apparent paradox: the dominant control on the core-melt and rim-melt trends involves little plagioclase crystallisation despite the fact that Mount St. Helens dacites have up to 35% plagioclase phenocrysts (Kuntz et al. 1981; Pearce et al. 1987). Conversely, the vector that connects the two groups of calculated melts is consistent with plagioclase-dominated crystallisation ($D_{Sr}^{bulk} >> D_{Ba}^{bulk}$). To reconcile these observations we suggest that the core and rim-melts are related to each other by a sudden change in crystallising assemblage from a plagioclase-poor assemblage to a plagioclase-rich assemblage, similar to that of the phenocrysts. Given the strong dependence of plagioclase stability on P_{H2O}, we infer that the plagioclase-poor assemblage corresponds to high P_{H2O}, while the plagioclase-rich assemblage corresponds to low P_{H2O}. The core-melts record the spectrum of compositions generated by crystallisation at high P_{H2O}, when plagioclase was a minor crystallising phase. As the melts ascend and encounter their vapour-saturated liquidus at lower P_{H2O} they become saturated with plagioclase (Annen et al. 2006). A sudden burst of plagioclase crystallisation will displace the core-melt trend to the rim-melt trend. Such a dramatic increase in plagioclase crystallisation is not recorded in the plagioclase phenocrysts that were studied, where the transition from core to rim is mostly recorded over a relatively short width (depending on crystal orientation). We suggest that this is a result of a rapid increase in the number of plagioclase crystals in the magma, rather than appreciable overgrowth of pre-existing phenocrysts. Consequently an individual plagioclase crystal experiences a dramatic drop in Sr and a slight increase in Ba in the surrounding melt without itself undergoing significant crystallisation. This process is illustrated schematically in Fig. 10. This hypothesis would also account for the simultaneous sudden change from ~An_{60} (zone 4) to ~An_{40} (zone 3) and the bimodal distribution of plagioclase compositions (Fig. 6). A further shift in melt composition is observed between the calculated rim-melts and the analysed groundmass/inclusion glasses (Fig. 9a). Once again the vector connecting these two groups is consistent with plagioclase-dominated crystallisation ($D_{Sr}^{bulk} >> D_{Ba}^{bulk}$). We propose that this crystallisation event corresponds to the growth of microlites. Blundy et al. (2007) use melt inclusion trace element chemistry and H_2O contents to infer two discrete crystallisation events, one at $P_{H2O} \approx 250$–150 MPa and the other at ≤ 70 MPa, which they ascribe to phenocrysts and microlites, respectively.

At least two shifts in Sr melt concentration are thus recorded: one links core-melts and rim-melts; the other links rim-melts and groundmass glasses from microlite-bearing samples. We suggest that these shifts are due to sudden increases in the proportion of plagioclase crystallising. Rapid crystallisation capable of depleting the surrounding melt in Sr can occur during both crystal growth-dominated (at low undercooling) and nucleation-dominated regimes (at high undercooling; e.g. Swanson 1977). Hammer and Rutherford (2002) show that for Mount Pinatubo dacite peaks in crystallisation rate were achieved at 100 MPa in a crystal growth-dominated regime and at 25 MPa in a nucleation-dominated regime. Although undercooling can be caused by various other processes, e.g. quenching and magma mixing, we suggest that decompression-driven degassing is the dominant process

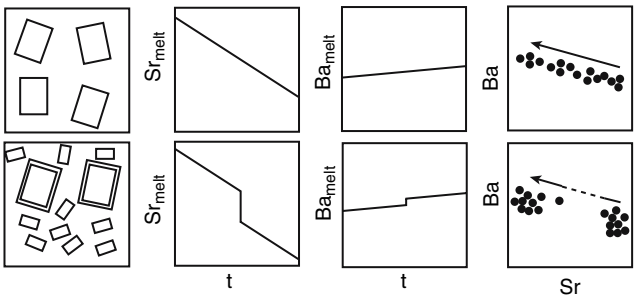

Fig. 10 Schematic illustration of the effect of nucleation on Sr and Ba concentrations in the melt. The *top set* of panels depicts normal crystallisation and therefore leads to smooth compositional variation, while the *bottom panels* illustrate the effect of rapid crystallisation due to plagioclase nucleation, which leads to a marked drop in Sr concentration in the melt with time. Because Ba is incompatible in plagioclase nucleation leads to only a modest increase in melt Ba concentration. Thus a nucleation event is identifiable in Sr–Ba space by a jump in Sr, but not in Ba

responsible for sudden plagioclase crystallisation at Mount St. Helens. Decompression crystallisation is widely cited as the main process responsible for microlite crystallisation in silicic magmas (Geschwind and Rutherford 1995; Cashman 1988, 1992; Blundy and Cashman 2001; Couch et al. 2003b; Hammer and Rutherford 2002). Some phenocryst crystallisation is also suggested to be the result of magma ascent (e.g. Kuritani 1999; Blundy and Cashman 2001). The slope of the H_2O-saturated dacite liquidus (e.g. Blundy and Cashman 2001) suggests that a large change in pressure at relatively high pressure will result in a much smaller undercooling than a similar change at lower pressure, assuming isothermal ascent. Thus crystallisation at high pressure will be dominated by crystal growth (resulting in a few phenocrysts), whereas at lower pressure the crystallisation will be nucleation dominated (resulting in many small microlites). Thus after crossing the H_2O-saturated liquidus at depth a few large, nearly homogeneous, euhedral, crystals will form. Type A cores often have a tabular shape, suggesting that they formed at small undercooling (e.g. Lofgren 1974a; Hammer and Rutherford 2002). Some may have nucleated on resorbed plagioclase (i.e. zone 5) that was already present in the magma during ascent from the source region. This burst of rapid crystal growth depletes the melt in Sr and Ca/Na (resulting in the sudden transition to low An plagioclase). Subsequent crystals grow from this depleted melt and thus have low Sr and lower An. A second depletion in Sr and An in the melt is caused by microlite crystallisation at shallower depths, where higher undercooling is attained. In both cases a relatively homogeneous crystal population is formed in a short time, leaving the melt depleted in compatible elements (i.e. Ca, Sr).

Type *B* crystals

Spongy cellular phenocrysts crystallised exclusively from the rim-melt (Fig. 9c). They are characterised by severe resorption of the core and extensive networks of connected melt channels that have become isolated at various stages during crystal growth. These melt inclusions provide a record of magmatic processes that has been exploited to infer the extent of decompression crystallisation (Blundy and Cashman 2005). The most H_2O- and CO_2-rich melt inclusions point to an entrapment depth of ~11 km below sea level (Blundy et al. 2007). Less H_2O-rich melt inclusions record the subsequent crystallisation that occurred during magma ascent. It can thus be inferred that the crystallisation responsible for the occlusion of melt inclusions was caused by decompression crystallisation. Since none of the observed melt inclusions recorded the core-melt (Fig. 9a), melt inclusion entrapment occurred only during the second step of crystallisation.

The cause of resorption resulting in the formation of the melt inclusion networks in type B crystals remains obscure. The resorption event that causes the spongy textures is likely to be the same event as that between zones 3 and 2, whereby resorption penetrated the crystals along weak zones such as fractures and cleavage planes. The resorption event thus predates the magma ascent that is recorded by the melt inclusions. The small change in plagioclase composition to higher An, and increase in calculated melt Sr concentration, that accompanies the resorption indicates that reheating with or without mixing-in of less evolved melts is a possibility.

Type *C* crystals

The texture described here as boxy cellular cores, with high An and a skeletal texture, has been attributed to both rapid crystal growth and to resorption (Kawamoto 1992; Nakamura and Shimakita 1998; Landi et al. 2004; Nelson and Montana 1992; Castro 2001; Izbekov et al. 2002). Under large undercooling irregular-shaped (e.g. hopper, swallow-tails, skeletal, etc.) crystals are formed (Lofgren 1974a; Hammer and Rutherford 2002). Such a process could explain the formation of the type C crystals. Later crystallisation (zones 4, 3, 2) may have resulted in filling-in of this irregular skeleton (zone 7), as demonstrated experimentally by Lofgren (1974b). The boxy cellular cores had a melt inclusion network similar to that of the spongy cellular cores, except that it was filled in extensively by plagioclase crystallisation leaving only few small melt inclusions trapped.

Izbekov et al. (2002) show that crystals from Karymsky volcano, which look similar to those at Mount St. Helens, result from interaction with a mafic melt. Their study benefits from the earlier eruption of closely related basalt, which contains calcic plagioclase similar to those observed in the subsequent andesite. At Mount St. Helens basalts were last erupted ~2,000 years ago during the Castle Creek period. Of the two basalts we have studied only the pre-Cave basalt could present a viable parent, because plagioclase from the Cave basalt has a much lower Sr concentration (Fig. 7). However Type C cores tend towards a euhedral rim and no obvious sign of a major resorption surface has been observed. The Mg concentration of zone 7 is also much lower that that of An rich plagioclase from either of the analysed basalts.

In some type C crystals the boxy cellular texture is also found surrounding a resorbed core, suggesting a dissolution and recrystallisation origin (Nakamura and Shimakita 1998; Landi et al. 2004). The high An plagioclase then crystallised onto of a pre-existing core, and the An-poor patches in the type C crystals (Figs. 1, 2) could be a combination of pre-existing resorbed core and later infill-

ing of the high An irregular rim. Chemically the An-poor patches (zone 6) are mostly derived from rim-melts, although some appear to be similar to type A core-melts (zone 4).

The boxy cellular cores (zone 7) form a poorly defined group that is quite unlike the rim- and core-melts (Fig. 9c). In fact the high Ba concentration of the melts from which these crystals appear to have crystallised has never been observed in magma erupted at Mount St. Helens (Fig. 9b). Magma with similar Ba and Sr concentration has, however, erupted at other Cascades volcanoes, e.g. Mount Jefferson (Conrey et al. 2000). Thus it is possible that small volumes of exotic magma are introduced into the Mount St. Helens system and homogenised prior to eruption, with only type C cores to testify to their presence. However type C cores do plot on an extension of the core trend formed by zones 4 and 5 (Figs. 4, 9c) suggesting that there is a possible relation.

Pre-1980 eruptions

Given the uncertainty about the eruption temperatures of the older magmas (Castle Creek, Sugar Bowl and Goat Rocks) and their most appropriate D_{Sr} and D_{Ba} equations, we have not sought to translate plagioclase Sr and Ba concentrations to melt concentrations. Nevertheless the 'core and 'rim' melts are indeed reflected in the plagioclase compositions (Fig. 4) and this figure can be compared to the plagioclase Sr and Ba concentrations in the pre-1980 plagioclase phenocrysts (Fig. 7).

The Goat Rocks andesite plagioclases have slightly lower Sr, but similar Ba to both the rims and cores from 1980, suggesting a similar two-stage ascent history. Sugar Bowl rhyodacitic plagioclase only has high Ba (corresponding to 1980 rim composition) and no low-Ba cores, although the two crystals that were analysed do have a sodic Ba-enriched mantle. Plagioclase phenocrysts of the Cave basalt (Castle Creek) show a similar trend to the 1980 cores, but at much lower Sr concentrations. This suggests that they have experienced a similar deep-seated, plagioclase-poor differentiation event, but were less fractionated consistent with their basaltic compositions and lower bulk-rock Sr concentration (Fig. 9b). As previously noted, the Pre-Cave basalt has similar Sr and Ba concentrations to the 1980 dacites.

Castle Creek-age cores in 1980 eruptions?

Cooper and Reid (2003) used U-series disequilibria to show that plagioclase phenocrysts from different eruptions spanning 2,000 years at Mount St. Helens are ≥2,000 years old and could thus have been present simultaneously. In this case the magma storage system was either made up of physically separated magma batches that were erupted sequentially or crystals of broadly similar age were entrained during each eruption. They speculate that some of the more recent eruptions could thus contain material that originated during the Castle Creek period, the only period during which basalt was erupted. The observed textural and chemical similarity between plagioclase phenocrysts from different ages would support such a scenario. Figure 5 also highlights the same wide compositional range of plagioclase phenocrysts erupted at different times despite variable bulk rock composition. For the one sample from the 1980–1986 eruption that was analysed by Cooper and Reid (2003), a 1982 dacite, the age of plagioclase crystallisation is undefined. This is explained by Cooper and Reid (2003) as possibly due to rapid crystallisation shortly before the eruption in accordance with the suggestion of Blundy and Cashman (2001, 2005) that part of the phenocryst crystallisation is due to decompression.

The interpretation of Cooper and Reid (2003), that a large portion of the phenocrysts grew only shortly before the eruption, is consistent with our results. The rims of the plagioclase phenocrysts (zones 1, 2, 3) are broadly in equilibrium with the groundmass melt composition of the 18 May eruption and some of the melt inclusions in subsequent eruptions (Blundy and Cashman 2005 and unpublished data; Fig. 9a). A significant portion of each crystal therefore appears to be relatively young and related to a sudden change in crystallisation conditions probably related to decompression and degassing of the magma. However, some cores of type A and C crystals could potentially be much older. The existence of a gap in the Sr concentration of the melt as recorded by cores and rims limits the age of the crystals to less than 10^4 years, because in very old crystals such a gap would not have been preserved due to diffusive reequilibration (Giletti and Casserly 1994). Detailed diffusion modelling will be needed to establish an age for the crystallisation of the rims.

The cores of the 1980 phenocrysts could date from the Castle Creek period, but it seems unlikely that they were derived from a basaltic parent. The calculated core-melt (Fig. 9b) at 900°C does not overlap with a basaltic bulk rock composition. However, basalts could have had much higher temperatures. Estimates for temperatures of Mount St. Helens basalts are given in Leeman et al. (2004) and vary between 1,186 and 1,213°C. Figure 9b shows the calculated core-melt at 1,200°C, which approaches basaltic compositions of Castle Creek age and overlaps with the 1980 bulk rock compositions. In further support of this argument, the two basalts from which plagioclase phenocrysts were analysed span a range of compositions similar to that of the 1980 plagioclases, albeit extending to higher

An. The low Sr concentrations in plagioclase from the Cave basalt discredits it as a viable parent melt, but the plagioclase in the pre-Cave basalt overlaps with plagioclase from 1980.

Despite the correspondence of Sr and Ba between plagioclase phenocrysts of the 1980 eruptions and those of one of the analysed basalts, however, this possibility is not viable for the following reasons. Firstly, the Mg concentration in 1980 plagioclase appears much too low for derivation from basalt. Secondly, the $^{87}Sr/^{86}Sr$ data from plagioclase in 1980 dacite argues against basalt involvement as all analyses have similarly high $^{87}Sr/^{86}Sr$, while published whole rock basalt data is uniformly low (Fig. 11). Thus it seems unlikely that type *A* plagioclase cores crystallised from a mafic melt despite their high An component. Instead we consider that the parent melt is likely to have been silicic. Crystallisation of An-rich plagioclase from an evolved melt origin requires conditions near the H_2O-saturated liquidus (e.g. Couch et al. 2001).

Magmatic processes

Deep storage

Figure 9 shows the plagioclase phenocrysts crystallised from melts that evolved towards higher Ba and Sr concentration indicating limited plagioclase in the crystallising assemblage of both. Published modal analyses of magma from the same eruptions suggest that plagioclase is by far the dominant phase, with 25–35% plagioclase, 2–4% amphibole, 3–6% orthopyroxene, 1–2 Fe–Ti oxide, <0.5% clinopyroxene (Cashman and Taggart 1983; Kuntz et al. 1981, Pearce et al. 1987). Fractional crystallisation with this mineral assemblage would result in a trend towards lower Sr and slightly higher Ba (Fig. 9a). Yet the variation in plagioclase cores indicates that the crystallising assemblage responsible for magma differentiation contained at most 23% plagioclase (An_{60}) and 77% other phases (with D_{Sr}~0). Thus, we propose that the plagioclase cores record an earlier, probably deeper, crystallisation event in which plagioclase itself was only a minor phase. This crystallisation event probably took place in a deep crustal hotzone as envisaged by Annen et al. (2006).

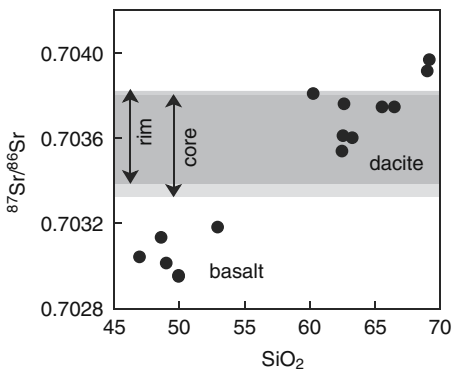

Fig. 11 $^{87}Sr/^{86}Sr$ variation in bulk rocks (data points from Leeman et al. 1990; Halliday et al. 1983) compared to that in selected plagioclase phenocrysts from the 18 May 1980 eruption. Plagioclase data overlap with evolved bulk rocks, but not with basalts. Note that even An-rich plagioclase (Table 1) does not have $^{87}Sr/^{86}Sr$ as low as in the basalts

Plagioclase is likely to be resorbed during magma ascent as long as the H_2O activity in the melt is less than unity (e.g. Nelson and Montana 1992; Annen et al. 2006) and it becomes a crystallising phase only when H_2O saturation is reached at shallower level in the plumbing system. Thus any plagioclase that is brought up from depth is expected to show some signs of resorption, except in the case of very rapid ascent. Yet the core-mantle transition (zones 4–3) does not show clear signs of resorption. The lack of resorption at the transition from core to mantle suggests that crystallisation was continuous or episodic, but not reversed.

H_2O-undersaturated magma ascending from deep in the crust would eventually encounter a depth at which plagioclase starts crystallising (e.g. Blundy and Cashman 2001; Carmichael 2002). If plagioclase is the principal liquidus phase at low pressure (Blundy and Cashman 2001) then the melt composition recorded by the plagioclase will be equivalent to that at the point of detachment from the source region in the lower crust. Thus, the compositional variation described by the core-melts (Fig. 9) is likely to reflect compositional variation generated by differentiation processes in the deep crust where fractionation of Sr and Ba poor phases (e.g. olivine, pyroxene, garnet) is dominant. This deep differentiation trend is defined by a large number of crystals; however no individual crystal records the entire observed variation to higher Sr and Ba concentration in the melt. This suggests that the cores record different batches of magma related to one another by fractionation of similar deep-seated mineral assemblages. The cores of 1980 plagioclase phenocrysts did not crystallise from a single batch of magma, but involved variably differentiated, individual batches from the same source, which accumulated at the point of plagioclase saturation at shallow pressure beneath the volcano (Fig. 12).

In this hypothesis the trend towards higher Sr and Ba concentrations in the core-melt is attributed to the lower crustal processes. In other words the melt differentiation recorded by the plagioclase cores pre-dates the actual growth of most plagioclase. After the initial burst of plagioclase crystallisation at low pressure the melt was left depleted in Sr. The parallel trend at lower Sr concentration of the rim-melts is thus displaced from the trend of the

core-melts by repeated crystallisation of individual magma batches to a similar degree. Our data are therefore consistent with the accumulation and crystallisation of sequential batches of magma generated in the lower crust, the Sr concentration of which is recorded upon plagioclase saturation (Fig. 12). Mass balance using the calculated melt Sr concentration from the cores as the initial melt composition and the 18 May groundmass Sr concentration (equivalent to the calculated melt composition of the rims), suggests that the amount of plagioclase that crystallised to create the gap between the core- and rim-melts in the data is ~15%.

Crystal mush/pluton

Since the plagioclase cores record related lower crustal melts of different degrees of fractionation they must have arrived in distinct batches of different compositions, to be accumulated in a shallow magma chamber. Thus type A cores, though ultimately derived from the same source, are not necessarily of the exact same age and not necessarily as old as the melt diversity they record. Repeated input of magma batches with similar composition and H_2O content would result in crystallisation of plagioclase over a small depth interval. This may have resulted in the formation of a plagioclase-rich crystal mush or ''proto-pluton'' (Pallister et al. 1992; Cooper and Reid 2003). Variations in the detailed zoning profiles of individual crystals may be ascribed to spatial and temporal variations within this proto-pluton. The bulk rock composition of the 1980 dacites does not overlap with any calculated melts, making it unlikely that they were ever true liquids. Rather the bulk rock appears to be a mixture of plagioclase and groundmass melt (Fig. 9a). The complex crystallisation history of any magma that formed under a range of pressure–temperature–time conditions and was a mixture of melt and plagioclase crystals, rather than a homogeneous melt will make the interpretation of experiments whereby such magma is remolten (e.g. Rutherford et al. 1985; Gardner et al. 1995b) challenging.

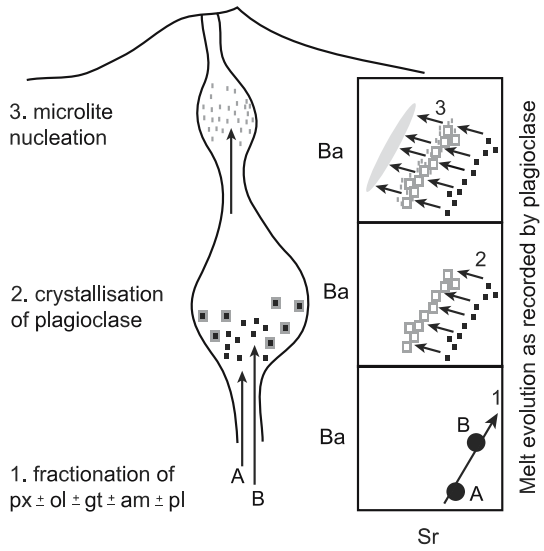

Fig. 12 Schematic summary of events recorded by plagioclase phenocrysts from the 1980 eruptions of Mount St. Helens. The *boxes* on the right hand side of the figure denote melt compositions. *1* Fractionation of a plagioclase-poor crystal assemblage in the deep crust leading to a spectrum of melt compositions (e.g. *A* and *B*) extending to high Ba and Sr concentration. *2* Rapid crystallisation of plagioclase after decompression-induced H_2O loss. After initial crystallisation burst crystals will try to re-equilibrate with the now degassed and Sr-depleted melt leading to a gap in Sr concentration. *3* Further magma ascent results in microlite crystallisation and causes a further drop in Sr concentration

Conclusions

The cores of plagioclase phenocrysts of the 1980 eruptions of Mount St. Helens reveal a differentiation trend in which plagioclase was a minor component, yet plagioclase is the most abundant phase in the erupted rock. This plagioclase-poor differentiation trend is inferred to result from crystallisation and melting during an early deep-seated stage of magma evolution, probably in the lower crust. Any plagioclase formed under these conditions is unlikely to have survived volatile undersaturated magma ascent. Consequently the differentiation trend has been preserved in plagioclase that crystallised only upon magma reaching volatile saturation at shallower depth. Thus the trend preserved in plagioclase cores is the result of the ascent of individual magma batches from a common deeper storage region, the Ba–Sr concentration of which became archived only when plagioclase re-appeared on the liquidus. The accumulation of individual magma batches in different stages of differentiation in a magma chamber at shallow depth thus accounts for the trend of increasing Sr and Ba observed in plagioclase.

Upon volatile saturation in the shallow magma chamber, a significant quantity of plagioclase will crystallise. After this initial burst of crystallisation, the melt is depleted in Sr and a gap in Sr concentration is recorded by the plagioclase. This is manifest as a marked compositional gap between core-melts and rim-melts. Similarly further magma ascent to even shallower levels, as evidenced from melt inclusion data (Blundy and Cashman 2005; Blundy et al. 2007), results in microlite crystallisation, which lowers the Sr concentration of the melt even further. The microlites, however, appear to record the melt concentration at the point of nucleation rather than the final groundmass composition, because the rim, which is in equilibrium with the groundmass, is too thin to analyse by SIMS. The record of

magmatic evolution as stored in the plagioclase archive thus reveals a multistage ascent and crystallisation history during which individual batches rise from a common storage region at depth to accumulate in a magma chamber. The bulk rock has a Sr concentration that is much higher than any of the Sr concentrations of the melts in equilibrium with the plagioclase suggesting that it was never a true liquid. Instead Mount St. Helens dacites appear to be mixtures of evolved melts and plagioclase crystals accumulated at shallow depths.

Acknowledgments We thank Stuart Kearns for help with EMP and SEM analyses at the University of Bristol, Simone Kasemann, Richard Hinton and John Craven for assistance on the SIMS, and Norm Pearson for help with laser ablation analysis at Macquarie University which is supported by the Australian Research Council and Department of Education Science and Training. We also thank Kathy Cashman, Jon Davidson, Catherine Ginibre, Steve Sparks, David Pyle, Gerhard Wörner, Vincent van Hinsberg and an anonymous reviewer for helpful comments. Access to the SIMS facility in Edinburgh was provided by the Natural Environment Research Council. During the course of this research KB was supported by a University of Bristol postgraduate scholarship and by the DEST through an Endeavour award; JB was supported through a NERC Senior Research Fellowship and ST by an Australian Federation Fellowship.

References

Adams CJ, Campbell HJ, Griffin WL (2005) Isotopic microanalysis of seawater strontium in biogenic calcite to assess subsequent rehomogenisation during metamorphism. Chem Geol 220:67–82

Albarède F, Bottinga Y (1972) Kinetic disequilibrium in trace element partitioning between phenocrysts and host lava. Geochim Cosmochim Acta 36:141–156

Allègre CJ, Provost A, Jaupart C (1981) Oscillatory zoning: a pathological case of crystal growth. Nature 294:223–229

Annen C, Blundy JD, Sparks RSJ (2006) The genesis of intermediate and silicic magmas in deep crustal hot zones. J Petrol 47:505–539

Berlo K, Blundy J, Turner S, Cashman K, Hawkesworth C, Black S (2004) Geochemical precursors to volcanic activity at Mount St. Helens, USA. Science 306:1167–1169

Bindeman IN, Bailey JC (1999) Trace elements in anorthite megacrysts from the Kurile island arc: a window to across-arc geochemical variations in magma compositions. Earth Planet Sci Lett 169:209–226

Bindeman IN, Davis AM, Drake MJ (1998) Ion- microprobe study of plagioclase-basalt partition experiment at natural concentration levels of trace elements. Geochim Cosmochim Acta 62:1175–1193

Blundy J, Cashman K (2001) Ascent driven crystallisation of dacite magmas at Mt. St. Helens. Contrib Miner Petrol 140:631–650

Blundy J, Cashman K (2005) Rapid decompression-driven crystallisation recorded by melt inclusions from Mount St. Helens volcano. Geology 33:793–796

Blundy JD, Shimizu N (1991) Trace element evidence for plagioclase recycling in calc-alkaline magmas. Earth Planet Sci Lett 102:178–196

Blundy JD, Wood BJ (1991) Crystal-chemical controls on the partitioning of Sr and Ba between plagioclase feldspar silicate melts and hydrothermal solutions. Geochim Cosmochim Acta 55:193–209

Blundy J, Cashman K, Humphreys M (2006) Magma heating by decompression-driven crystallization beneath andesite volcanoes. Nature 443:76–80

Blundy J, Cashman K, Berlo K (2007) Evolving Magma Storage Conditions beneath Mount St. Helens Inferred from Chemical Variations in Melt Inclusions from the 1980–1986 and Current Eruptions. US Geol Surv Prof Pap (in press)

Carmichael ISE (2002) The andesite aqueduct: perspectives on the evolution of intermediate magmatism in west-central (105-99°W) Mexico. Contrib Miner Petrol 143:641–663

Cashman K (1992) Groundmass crystallisation of Mt St. Helens dacite, 1980–1986: a tool for interpreting shallow magmatic processes. Contrib Miner Petrol 109:431–449

Cashman KV (1988) Crystallisation of Mount St. Helens 1980–1986 dacite: a quantitative textural approach. Bull Volcanol 50:194–209

Cashman KV, Taggart JE (1983) Petrologic monitoring of 1981–1982 eruptive products from Mount St. Helens, Washington. Science 221:1385–1387

Cashman KV, Hoblitt RP (2004) Magmatic precursors to the 18 May 1980 eruption of Mount St. Helens, USA. Geology 32:141–144

Castro A (2001) Plagioclase morphologies in assimilation experiments, implications for disequilibrium melting in the generation of granodiorite rocks. Miner Petrol 71:31–49

Conrey RM, Hooper PR, Larson PB, Chesley J, Ruiz J (2000) Trace element and isotopic evidence for two types of crustal melting beneath a High Cascade volcanic center, Mt. Jefferson, Oregon. Contrib Miner Petrol 141:710–732

Cooper KM, Reid MR (2003) Re-examination of crystal ages in recent Mount St. Helens lavas: implications for magma reservoir processes. Earth Planet Sci Lett 213:149–167

Couch S, Sparks RSJ, Carroll MR (2001) Mineral disequilibrium in lavas explained by convective self-mixing. Nature 411:1037–1039

Couch S, Harford CL, Sparks RSJ, Carroll MR (2003a) Experimental constraints on the conditions of formation of highly calcic plagioclase microlites at the Soufrière Hills volcano, Montserrat. J Petrol 44:1455–1475

Couch S, Sparks RSJ, Carroll MR (2003b) The kinetics of degassing-induced crystallization at Soufrière Hills volcano, Montserrat. J Petrol 44:1477–1502

Criswell CW (1987) Chronology and pyroclastic stratigraphy of the May 18, 1980, eruption of Mount St. Helens, Washington. J Geophys Res 92:10237–10266

Davidson JP, Hora JM, Garrison JM, Dungan MA (2005) Crustal forensics in arc magmas. J Volcanol Geother Res 140:157–170

Gardner JE, Carey S, Rutherford MJ, Sigurdsson H (1995a) Petrologic diversity in Mount St. Helens dacites during the last 4,000 years: implications for magma-mixing. Contrib Miner Petrol 119:224–238

Gardner JE, Rutherford M, Carey S, Sigurdsson H (1995b) Experimental constraints on pre-eruptive water contents and changing magma storage prior to explosive eruptions of Mount St. Helens volcano. Bull Volcanol 57:1–17

Gardner JE, Layer PW, Rutherford MJ (2002) Phenocrysts versus xenocrysts in the youngest Toba Tuff: Implications for the petrogenesis of 2,800 km^3 of magma. Geology 30:347–350

Geschwind C-H, Rutherford MJ (1995) Crystallisation of microlites during magma ascent: the fluid mechanics of 1980–1986 eruptions at Mount St. Helens. Bull Volcanol 57:356–370

Giletti BJ, Casserly JED (1994) Strontium diffusion kinetics in plagioclase feldspars. Geochim Cosmochim Acta 58:3785–3793

Ginibre C, Wörner G, Kronz A (2002) Minor and trace element zoning in plagioclase: implications for magma chamber pro-

cesses at Parinacota volcano, northern Chile. Contrib Miner Petrol 143:300–315
Halliday AN, Fallick AE, Dickin AP, Mackenzie AB, Stephens WE, Hildreth W (1983) The isotopic and chemical evolution of Mount St. Helens. Earth Planet Sci Lett 63:241–256
Hammer JE, Rutherford MJ (2002) An experimental study of the kinetics of decompression-induced crystallisation in silicic melt. J Geophys Res 107 B1 ECV 8:1–24
Hawkesworth CJ, Blake S, Evans P, Hughes R, Macdonald R, Thomas LE, Turner SP, Zellmer G (2000) Time scales of crystal fractionation in magma chambers-Integrating physical, isotopic and geochemical perspectives. J Petrol 41:991–1006
Irving AJ, Frey FA (1984) Trace element abundances in megacrysts and their host basalt-constraints on partition-coefficients and megacryst genesis. Geochim Cosmochim Acta 48:1201–1221
Izbekov PE, Eichelberger JC, Patino LC, Vogel TA, Ivanov BV (2002) Plagioclase cores of plagioclase phenocrysts in andesite from Karymsky volcano: evidence for rapid introduction of basaltic replenishment. Geology 30(9):799–802
Kawamoto T (1992) Dusty and honeycomb plagioclase: indicators of processes in the Uchino stratified magma chamber. J Volcanol Geotherm Res 49:191–208
Kuntz MA, Rowley PD, MacLeod NS, Reynolds RL, MacBroome LA, Kaplan AM, Lidke DJ (1981) Petrography and particle-size distribution of pyroclastic-flow, ash-cloud, and surge deposits. US Geol Surv Prof Pap 1250:525–539
Kuritani T (1999) Phenocryst crystallisation during ascent of alkali basalt magma at Rishiri Volcano, northern Japan. J Volcanol Geotherm Res 88:77–97
Landi P, Métrich N, Bertagnini A, Rosi M (2004) Dynamics of magma-mixing and degassing recorded in plagioclase at Stromboli (Aeolian Archipelago, Italy). Contrib Mineral Petrol 147:213–227
Leeman WP, Smith DR, Hildreth W, Palacz Z, Rogers N (1990) Compositional diversity of Late Cenozoic basalts in a transect across the southern Washington Cascades: implications for subduction zone magmatism. J Geophys Res 95:19561–19582
Leeman WP, Lewis JF, Evarts RC, Conrey RM, Streck MJ (2004) Petrologic constraints on the thermal structure of the Cascades arc. J Volcanol Geotherm Res 140:67–105
Lofgren G (1974a) An experimental study of plagioclase crystal morphology: isothermal crystallization. Am J Sci 274:243–273
Lofgren G (1974b) Temperature induced zoning in synthetic plagioclase feldspar. In: MacKenzie WS, Zussman J (eds) The feldspars. Manchester University Press, Manchester, pp 362–375
Melson WG (1983) Monitoring the 1980–1982 eruptions of Mount St. Helens: compositions and abundances of glass. Science 221:1387–1391
Morgan GB VI, London D (2003) Trace-element partitioning at conditions far from equilibrium: Ba and Cs distribution between alkali feldspar and undercooled hydrous granitic liquid at 200 MPa. Contrib Miner Petrol 144:722–738
Morse SA (1984) Cation diffusion in plagioclase feldspar. Science 225:504–505
Nakamura M, Shimakita S (1998) Dissolution origin and syn-entrapment compositional change of melt inclusions in plagioclase. Earth Planet Sci Lett 161:119–133
Nelson ST, Montana A (1992) Sieve-textured plagioclase in volcanic rocks produced by rapid decompression. Am Miner 77:1242–1249
Pallister JS, Hoblitt RP, Crandell DR, Mullineaux DR (1992) Mount St. Helens a decade after the 1980 eruptions: magmatic models, chemical cycles and a revised hazards assessment. Bull Volcanol 54:126–146
Pearce TH, Russell JK, Wolfson I (1987) Laser-interference and Nomarski interference imaging of zoning profiles in plagioclase phenocrysts from the May 18, 1980, eruption of Mount St. Helens, Washington. Am Miner 72:1131–1143
Rutherford MJ, Hill PM (1993) Magma ascent rates from amphibole breakdown: an experimental study applied to the 1980–1986 Mount St Helens eruption. J Geophys Res 98:19667–19685
Rutherford MJ, Sigurdsson H, Carey S, Davis A (1985) The May 18, 1980, eruption of Mount St. Helens 1. Melt composition and experimental phase equilibria J Geophys Res 90:2929–2947
Singer BS, Dungan MA, Layne GD (1995) Textures and Sr, Ba, Mg, Fe, K, and Ti compositional profiles in volcanic plagioclase: clues to the dynamics of calc-alkaline magma chambers. Am Miner 80:776–798
Smith DR (1984) The petrology and geochemistry of high Cascade volcanics in southern Washington: Mount St Helens volcano and the Indian Heaven basalt field. PhD thesis, Rice University, p 409
Smith DR, Leeman WP (1987) Petrogenesis of Mount St. Helens dacitic magmas. J Geophys Res 92:10313–10334
Smith DR, Leeman WP (1993) The origin of Mount St. Helens andesites. J Volcanol Geotherm Res 55:271–303
Stamatelopoulou-Seymour K, Vlassopoulos D, Pearce TH, Rice C (1990) The record of magma chamber processes in plagioclase phenocrysts at Thera volcano, Aegean volcanic arc. Contrib Miner Petrol 104:73–84
Stewart ML, Pearce TH (2004) Sieve textured plagioclase in dacitic magma: Interference imaging results. Am Miner 89:348–351
Swanson SE (1977) Relation of nucleation and crystal-growth rate to the development of granitic textures. Am Miner 62:966–978
Tepley III FJ, Davidson JP, Tilling RI, Arth JG (2000) Magma mixing, recharge and eruption histories recorded in plagioclase phenocrysts from El Chichon volcano, Mexico. J Petrol 41:1397–1411
Tsuchiyama A (1985) Dissolution kinetics of plagioclase in the melt of the system diopside-albite-anorthite, and the origin of dusty plagioclase in andesites. Contrib Miner Petrol 89:1–16
Turner S, George R, Jerram DA, Carpenter N, Hawkesworth C (2003) Case studies of plagioclase growth and residence times in island arc lavas from Tonga and the Lesser Antilles, and a model to reconcile discordant age information. Earth Planet Sci Lett 214:279–294
Vander Auwera J, Longhi J, Duchesne JC (2000) The effect of pressure on DSr (plag/melt) and DCr (opx/melt): implications for anorthosite petrogenesis. Earth Planet Sci Lett 178:303–314